In-Depth Study into the Interaction of Single Walled carbon Nanotubes with Anthracene and *p*-Terphenyl

Theresa G. Hedderman,* Sinead M. Keogh, Gordon Chambers, and Hugh J. Byrne

Focas Institute/School of Physics, Dublin Institute of Technology, Kevin Street, Dublin 8, Ireland

Received: October 4, 2005; In Final Form: December 2, 2005

Solubilization of single walled carbon nanotubes (SWNT) in the presence of polycyclic aromatic hydrocarbons (PAHs) such as *p*-terphenyl and anthracene has been shown. The suspensions formed are stable for periods greater than 48 months but to date experimental research is scarce regarding the interactions that are taking place. Spectroscopic analysis such as Raman and fluorescence are used to probe the interactions occurring between the PAHs and the SWNT over a wide concentration range. Previous studies show the fluorescence of the PAHs is quenched on interaction with SWNT and in the case of *p*-terphenyl, the spectrum is red shifted. This result prompted a study of a large range of concentrations to quantify the degree of interaction between the SWNT and PAHs. It was found at high concentrations that both the PAHs and SWNT formed aggregates and at lower concentrations it was found that free PAHs and isolated SWNT were interacting. The radial breathing modes (RBMs) in Raman spectroscopy gave detail as to how diameter selective the PAH samples are when compared to the pristine SWNT modes. An increase in the wavenumber of the RBMs for both composite spectra was observed and it is believed that such a result is due to the debundling of the SWNT on interaction with the PAHs. It was also found that anthracene and *p*-terphenyl selectively interact with SWNT and the selected SWNT were found to be within a distinct diameter range and possessed unique physical properties.

Introduction

Single walled carbon nanotubes (SWNT) have generated much interest due to their unique properties and potential for application.[1−4] There are, however, some fundamental problems that need to be addressed. As a result of the production process, not only are SWNT samples impure but also they are almost always present in the form of bundles with the properties of the bundle inferior to that of individual SWNT.[5−9] For application purposes it is necessary to have access to isolated SWNT where particular electronic characteristic may be routinely selected. Polycyclic aromatic hydrocarbons (PAHs) such as anthracene and *p*-terphenyl have been used to address issues of solubility and purification.[10] It was found that both *p*-terphenyl and anthracene solubilized SWNT and that suspensions formed were stable for periods greater than 48 months. It was also shown that the PAHs purified the SWNT sample by interacting and suspending only SWNT. It has been proposed that due to the differing structure of anthracene and *p*-terphenyl, they may potentially interact with specific SWNT.[10] Anthracene was proposed to map onto metallic SWNT and *p*-terphenyl to mainly semiconducting SWNT and this study investigates such a proposal. This proposal is based on the commensurate stacking of PAHs on graphene structures.[11] Experimental research to date is scarce regarding the interaction that occurs between PAHs and SWNT; however, the aim of this paper is to probe such interactions through spectroscopic methods such as fluorescence and Raman.

* Corresponding author. Ph: 00 353 1 402 7907, Fax: 00 353 1 402 7904. E-mail: theresa.hedderman@dit.ie.

Experimental Section

Solutions of the PAHs, *p*-terphenyl and anthracene in toluene were prepared. The concentrations prepared were between $\sim 2.5 \times 10^{-3}$ and $\sim 4.5 \times 10^{-12}$ M for *p*-terphenyl and $\sim 3.0 \times 10^{-3}$ and $\sim 3.0 \times 10^{-9}$ M for anthracene. The PAHs solutions were characterized using UV−vis−NIR (Perkin-Elmer Lambda 900), fluorescence (Perkin-Elmer LS55) and Raman spectroscopy (Instruments SA LabRam 1B). Laser vaporization SWNT obtained from Rice University (Tubes@rice, Houston, TX) were added to all dye solutions in a 1:1 ratio by weight (w/w) SWNT/PAH molecules.

All suspensions were sonicated using a Branson ultrasonic tip for 30 s and allowed to settle for 24 h, after which the supernatant liquid was carefully decanted. In all cases the suspensions were then allowed to settle for a further 24 h before being characterized by the various spectroscopic methods mentioned above. The precipitate was found to be relatively rich in SWNT so solubilization is only partial. Throughout this paper all the dispersion concentrations quoted are as prepared. For Raman measurements at 632.8 nm samples were dispersed on an activated silicon slide.[12,13] The silicon wafer was activated by covering the slide in a layer of (3-aminopropyl)triethoxysilane (APTES) for 10 min, after which the slide was rinsed with deionized water and dried at room temperature.[12,13] The activated slide was then immersed in the composite solution for approximately 3 weeks. Once removed from solution, the slide was rinsed with deionized water and allowed to dry at room temperature before being characterized.

Results and Discussion

Figure 1 shows the fluorescence of *p*-terphenyl in the absence (filled black circles) and presence (filled gray squares) of SWNT

10.1021/jp055647q CCC: $33.50
Published on Web 02/10/2006

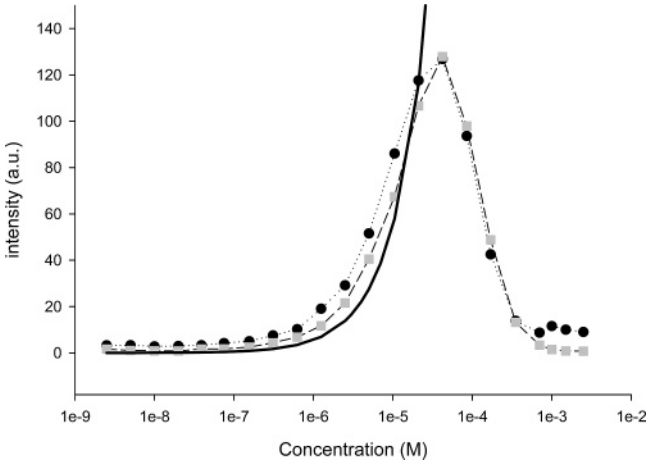

Figure 1. Fluorescence of *p*-terphenyl in the absence (filled black circles) and presence of SWNT (filled gray squares) as a function of concentration on a linear/log axis. The solid black line represents a linear fit to the data. Deviation from the fit is as a result of aggregation of the PAH molecules.

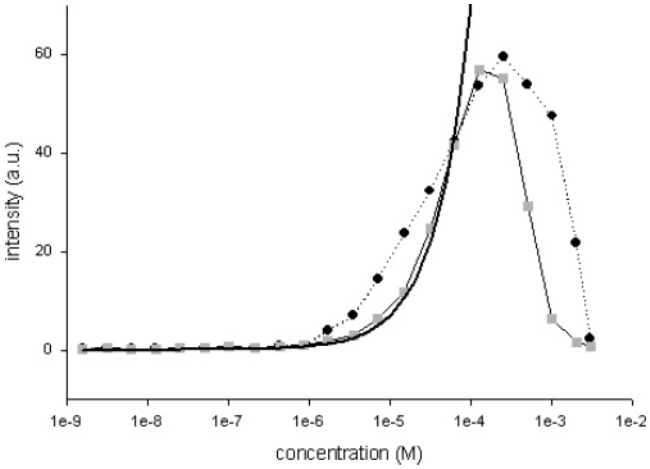

Figure 2. Fluorescence of anthracene in the absence (filled black circles) and presence of SWNT (filled gray squares) as a function of concentration on a linear/log axis. The solid black line represents a linear fit to the data. Deviation from the fit is a result of aggregation of the PAH molecules.

at concentrations between $\sim 2.5 \times 10^{-9}$ and $\sim 2.5 \times 10^{-3}$ M. For *p*-terphenyl (filled black circles) the concentration dependence of the fluorescence fits well to a linear increase between $\sim 2.5 \times 10^{-9}$ and $\sim 1 \times 10^{-5}$ M denoted by the black solid line. Note the plot is depicted in a linear/log axes. From $\sim 4.2 \times 10^{-5}$ to $\sim 7 \times 10^{-4}$ M the fluorescence deviates from linearity, and this deviation is evident both at the spectral maximum and on the red side of the spectrum, indicating that it is not due to reabsorption. The deviation may be attributed to the formation of aggregates of *p*-terphenyl, which causes quenching of the fluorescence.

Upon the addition of SWNT (filled gray squares) to the *p*-terphenyl solutions, the fluorescence trend of the composite solutions appears similar to that of the *p*-terphenyl discussed above. Between $\sim 2.5 \times 10^{-9}$ and $\sim 2 \times 10^{-5}$ M the fluorescence of the composite is linear but quenched relative to *p*-terphenyl. At approximately $\sim 3 \times 10^{-5}$ M the fluorescence of the composite deviates from linearity, but relative to *p*-terphenyl the fluorescence of the composite is now in excess. The additional fluorescent intensity observed may be explained by the destacking of the PAH aggregates. The fluorescence data appear to suggest that the addition of SWNT interferes with and hinders the aggregation process of *p*-terphenyl. This affect on aggregation indicates that the *p*-terphenyl preferentially interacts with SWNT and suggests that the binding energy of *p*-terphenyl/SWNT is higher than the binding energy of *p*-terphenyl/*p*-terphenyl. This suggestion is not unreasonable because theoretically binding energy calculations and thermal desorption studies discussed later in this paper for graphite and PAHs show that the PAH/graphite interaction is more favorable than the PAH/PAH interaction.[14−16]

Figure 2 depicts the fluorescence of anthracene in the absence (filled black circles) and presence of SWNT (filled gray squares), and its profile is similar to Figure 1. An interesting point to note, however, is that the point of aggregation for anthracene is found in the region of $\sim 2.5 \times 10^{-4}$ M. This is approximately a factor of 10 greater than the aggregation region of *p*-terphenyl, Figure l. Such a result is to be expected, as theoretical calculations predict that, as the number of carbons in PAHs increases, so too does the binding energy, which is expressed by the formation of aggregates at lower concentrations.[14−16] In the case of the *p*-terphenyl composite, excess fluorescence was indicative of the SWNT interference with aggregation, but for the anthracene composite, this region is not as distinct. Evidence of where this process begins can be seen in the region of $\sim 1 \times 10^{-4}$ M, but otherwise quenching is observed. This result may indicate that, when the anthracene aggregates are dispersed by the SWNT, the free anthracene appears to interact with surrounding SWNT, so that quenching is observed, whereas it would appear that *p*-terphenyl preferentially remains free in solution, so that excess fluorescence is observed. *p*-Terphenyl is a longer molecule than anthracene, with lengths of 1.15 and 0.72 nm, respectively; therefore fewer *p*-terphenyl molecules compared with anthracene can map to the SWNT surface of the same size, thus offering one possible explanation of the observed data.

Theoretical models based on the interaction of PAHs with themselves and graphite have been described in the literature.[14−16] The binding energies for PAH dimers and PAH/graphite were calculated using methods such as van der Waals density functional, Hartree−Fock and Redhead to name a few. The structure of a SWNT is essentially a curved single layer of graphite, and these structures are commonly found in bundles. The quasi crystalline arrangements of close packed SWNT like graphite, are held together by a long-range van der Waals interaction. With both graphite and SWNT possessing similar properties, it is reasonable to expect similar degrees of interaction for SWNT with PAHs. Theoretical models predict and thermal desorption spectroscopy confirm that an increase in the carbon number of PAHs increases the binding energy between PAHs, with larger PAH having similar interlayer distances and binding energies to graphite.[14−16] The binding energy between PAH and graphite is predicted to be larger than the binding energy of a corresponding PAH dimer. For example, the binding energy of benzene and naphthalene on a graphite surface were calculated to be 0.5 and 0.9 eV, respectively, compared with 0.1 and 0.17 eV for the respective dimers.[14,15] With current available theoretical and experimental data, it is reasonable to predict that the SWNT/PAH binding energy will be greater than the PAH/PAH binding energy and this is currently observed in Figures 1 and 2.

Coleman et al., constructed a model based on adsorption/desorption equilibrium of SWNT and polymers based on quenching of the fluorescence of the organic polymer when bound to the SWNT.[6] From this an indirect measurement of the polymer/SWNT binding energy and an elucidation of the

binding scheme could be achieved. The ratio of the maximum fluorescence intensity of the composite sample, which contains bound and unbound polymer, and the maximum fluorescence of the polymer, which solely comprises of unbound polymer chains, was plotted as a function of concentration. The model presented was for low concentrations, and when the system is in equilibrium, the adsorption rate equals the desorption rate. The adsorption rate was calculated theoretically; representing a SWNT (or bundle) as a cylinder and assuming that any molecule that reaches the SWNT adsorbs via van der Waals interactions. The desorption rate was shown to follow first-order kinetics and was calculated as a function of the number of bound molecules per unit volume, the volume of solution occupied by one SWNT. As the fraction of free polymer changed over the concentration range studied, a relationship was derived whereby the change in the fraction of free polymer could be described by a characteristic concentration C_0 and SWNT concentration $C_{NT.}$ Determination of the characteristic concentration allows the indirect measurement of the polymer/SWNT binding energy, and an elucidation of the binding scheme can be achieved.

Equation 1 represents the equilibrium at which the adsorption rate equals the desorption rate, where N_F is the number of free molecules, N_B is the number of bound molecules, Fl_{comp} is the

$$N_F/(N_F + N_B) = 1/(1 + C_{NT}/C_0) = Fl_{comp}/Fl_{polymer} \quad (1)$$

fluorescence of the composite and $Fl_{polymer}$ is the fluorescence of the polymer which gives the fraction of free polymer in solution. The model was derived for 1:1 ratios by mass and so for all concentrations the partial SWNT concentration, C_{NT}, equals the partial polymer concentration, C_p.

The study demonstrated that the model was well behaved in 1:1 composites by weight up to concentrations of 1×10^{-7} kg/m^3 in the case of the polymer composites and yielded a single value for characteristic concentration (C_0) of 2.2×10^{-5} kg/m^3.[6] A binding energy of 1.1 eV per molecule of poly[*m*-phenylenevinylene-*co*-(1,5-dioctyl-2,6-naphthlenylvinylene)] (pmNV) was calculated. Deviation from the ideal behavior was shown to result from changes in the SWNT size and therefore bundle size, and as a result, the model was thus able to elucidate concentration ranges in which the polymer interacted with the SWNT individually and in bundles of varying diameter.

Adapting this model and using the data from Figures 1 and 2 and applying eq 1, a plot of the fraction of free dye as a function of concentration was achieved, as shown in Figures 3 and 4. From the discussion above and Figure 1, *p*-terphenyl exists as nonaggregated molecules only below $\sim 2 \times 10^{-5}$ M (4.6×10^{-3} kg/m^3). Between $\sim 2 \times 10^{-5}$ M (4.6×10^{-3} kg/m^3) and $\sim 1 \times 10^{-8}$ M (2.3×10^{-6} kg/m^3) in Figure 3, the quenching of the fluorescence represents a decrease in the fraction of free *p*-terphenyl. In this concentration range the free *p*-terphenyl molecules interact with SWNT bundles causing debundling and forming stable suspensions. As described in the literature and this paper, the SWNT bundle size decreases with decreasing concentration until a transition region is reached where the SWNT bundles disperse to give isolated SWNT.[6] The concentration at which this occurs for *p*-terphenyl in this study is in the region of $\sim 3 \times 10^{-9}$ M (6.9×10^{-7} kg/m^3) and $\sim 6 \times 10^{-9}$ M (1.4×10^{-6} kg/m^3). From this point to approximately $\sim 4 \times 10^{-12}$ M (9.2×10^{-10} kg/m^3), the isolated PAHs and SWNT exist in a dynamic equilibrium with bound PAHs and nanotubes. The solid line in Figure 3 is a plot of eq 1 in this concentration range. The optimum calculated C_0 value was estimated to be $\sim 4 \times 10^{-10}$ M (9.2×10^{-8} kg/m^3). An important point to mention is that, in the dynamic equilibrium concentration range, the fluorescence was found to exceed 1.0. This is assumed to be the result of a background effect due to the SWNT, which will be discussed further.[17]

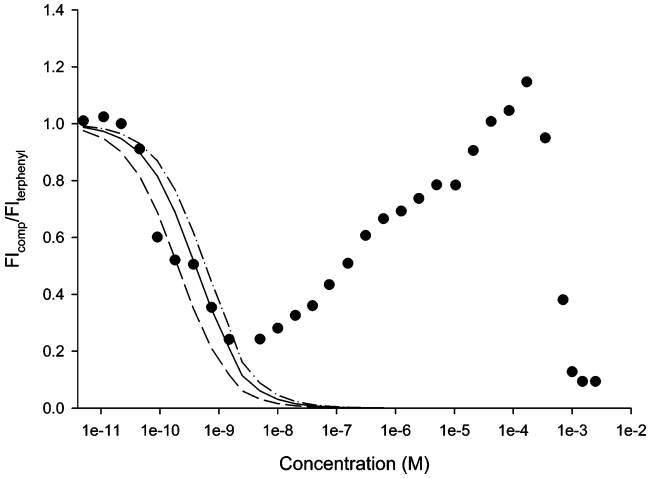

Figure 3. Graph of the fraction of free *p*-terphenyl as a function of concentration. The solid line is a fit to eq 1. The black solid line gives a C_0 value of $\sim 4 \times 10^{-10}$ M and the best fit to the data. To the left of the solid line, the dashed line gives a C_0 value of $\sim 2 \times 10^{-10}$ M, and to the right of the solid line, the dashed dotted line gives a C_0 value of $\sim 6 \times 10^{-10}$ M.

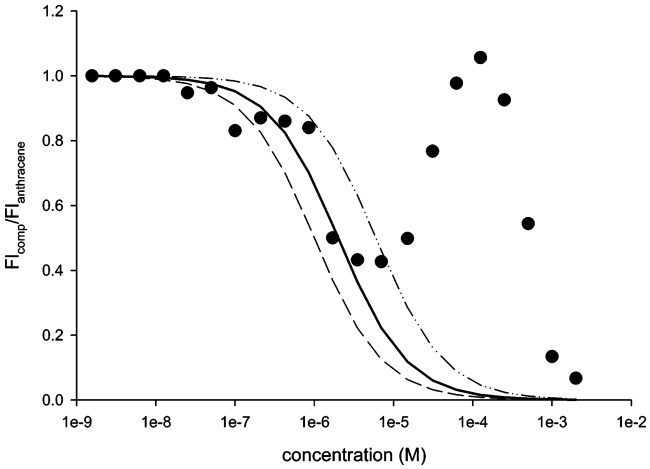

Figure 4. Fraction of free anthracene as a function of concentration. The solid line is a fit to eq 1.The black solid line gives a C_0 value of $\sim 2 \times 10^{-6}$ M and the best fit to the data. To the left of the solid line, the dashed line gives a C_0 value of $\sim 1 \times 10^{-6}$ M, and to the right of the solid line, the dashed dotted line gives a C_0 value of $\sim 6 \times 10^{-6}$ M.

In Figure 4 concentrations between $\sim 3 \times 10^{-3}$ M (5.3×10^{-1} kg/m^3) and $\sim 1 \times 10^{-4}$ M (1.8×10^{-2} kg/m^3) represent aggregated anthracene and SWNT bundles. Between $\sim 1 \times 10^{-4}$ M (1.8×10^{-2} kg/m^3) and $\sim 7 \times 10^{-6}$ M (1.3×10^{-3} kg/m^3) the graph depicts a monotonic decrease in the fraction of free anthracene. In this concentration range, the free anthracene molecules interact with SWNT bundles, causing debundling and forming stable suspensions. The transition region between bundles and isolated SWNT in this study is $\sim 3.5 \times 10^{-6}$ M (6.2×10^{-4} kg/m^3), and from this point to $\sim 1 \times 10^{-9}$ M (1.8×10^{-7} kg/m^3) the isolated dye molecules and SWNT exist. The solid line in Figure 4 is a plot of eq 1 in this concentration range with the C_0 value estimated at $\sim 2 \times 10^{-6}$ M (3.6×10^{-4} kg/m^3). This value is considerably higher compared to the value obtained for the *p*-terphenyl, so it would appear that anthracene is more prolific at dispersing SWNT bundles. This may be due to the planar structure of anthracene, as its rigid, planar structure

allows relatively easy intercalation between bundles and, once there, it may act as a nanospacer and disperses the bundled SWNT. *p*-Terphenyl is not a planar molecule and its three phenyl rings are rotated[18] with respect to each other, therefore making it more difficult for *p*-terphenyl to penetrate the SWNT bundle and disperse the nanotubes within the bundle.

$$C_0 = \pi^2 \upsilon \rho_{bun} A_{bun} e^{-E_B/kT}/(48Df) \quad (2)$$

In eq 2, υ represents the preexponential factor and was calculated to be $\sim 10^{18}$ Hz and ρ_{bun} is the bundle mass density that was calculated to be 1.33×10^3 kg/m^3 for Laser vaporization SWNT and E_B is the binding energy.[6,15,19] Other parameters such as the diffusion coefficient (D) for the *p*-terphenyl composite and for the anthracene composite were calculated to be 7.3×10^{-10} and 1.2×10^{-9} m^2/s respectively; f and A_{bun} are a space integral and the bundle surface area, which were calculated to be 800 and 3.6×10^{-6} m^2, respectively.[6,19] Using eq 2 and the C_0 values from Figures 3 and 4, the binding energies for both anthracene and *p*-terphenyl to the SWNT were calculated. It was found that C_0 is proportional to the inverse exponent of E_B. The point of deviation of the model from the data appears inversely related to the binding energy, and the polymer charaterized in ref 6 follows this trend. The C_0 value for *p*-terphenyl is 9.2×10^{-8} kg/m^3, anthracene is 3.6×10^{-4} kg/m^3 and pmNV is 4×10^{-6} kg/m^3, giving binding energies of 1.1, 0.9 and 1.1 eV, respectively. A true comparison of results obtained for anthracene and *p*-terphenyl in this study to the polymer pmNV from ref 6 cannot be made, as different systems are involved. The system studied in ref 6 is composed of chloroform, Hipco SWNT and pmNV, and the systems studied here are composed of toluene, laser vaporization SWNT and small organic molecules; different systems will affect the C_0 value and consequently the E_B. However, from the results it may be deduced that in the region of isolated SWNT, with increasing concentration, the higher energy molecule interacts with SWNT at lower concentrations. Thus with decreasing concentration, the higher energy molecules interact more strongly with the bundle surfaces and is less effective in intercalating and dispersing the tubes.

Contrary to that stated by Coleman et al., this study shows that, when the E_B is calculated,the C_0 value is not a constant even when SWNT from the same batch are used.[6] The model by Coleman et al. is limited in that the C_0 value calculated using atomic force microscopy (AFM) measurements and the model was used to elucidate the E_B of two different systems: one containing pmNV and the second containing poly[*p*-phenylenevinylene-*co*-(1,5-dioctyl-2,6-naphthlenylvinylene)] (ppNV).[6] It has been shown in this study that different molecules affect the point at which SWNT disperse and interact with SWNT and therefore result in a unique C_0 value. The studies conducted in this paper emphasize the need to calculate a new C_0 value each time a new molecule is introduced to the system and that it is not simply sufficient to calculate a single C_0 value and apply it to different systems. What is evident from the studies above is that anthracene is more prolific at dispersing SWNT bundles but *p*-terphenyl has a higher binding energy, a result supported both theoretically and experimentally in this paper.[14−16]

In a previous paper it was described how *p*-terphenyl on interaction with SWNT showed a red shift in fluorescence by 20 nm, but *p*-terphenyl alone at the specified concentrations did not.[10] This result was further explored at concentrations ranging from $\sim 2.5 \times 10^{-9}$ to $\sim 5 \times 10^{-3}$ M were the SWNT to PAH ratio was a 1:1 w/w. The results are displayed in Figure 5, and it would appear that there is no apparent red shift of

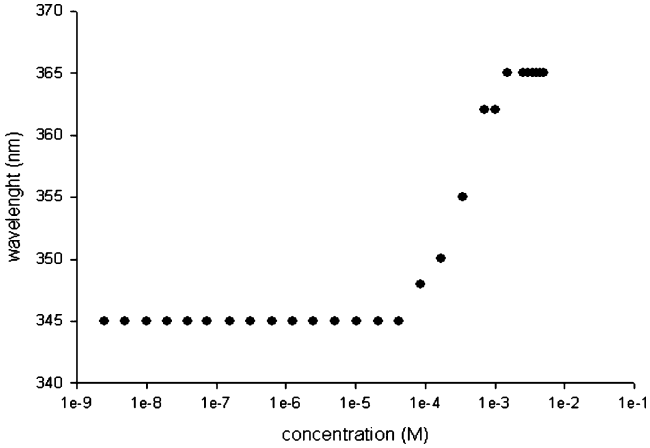

Figure 5. Red shift of the *p*-terphenyl emission maximum as a function of concentration in the presence of SWNT at a 1:1 ratio w/w.

p-terphenyl up to concentrations of $\sim 3 \times 10^{-5}$ M. From this point, red shifting was observed to increase with increasing concentration and a plateau was reached at $\sim 1 \times 10^{-3}$ M. The findings in Figure 5 raised a number of questions. The first was whether the red shift was indicative of the degree of interaction. This notion was eliminated through fluorescence and Raman spectroscopy, as quenching in fluorescence of *p*-terphenyl was observed below $\sim 1 \times 10^{-4}$ M and Raman detected the presence of SWNT below this concentration, thus signifying interaction. Literature states that the red shift of *p*-terphenyl is as a result of the three phenyl rings of the PAH molecules aligning themselves and mapping parallel to the SWNT surface,[18] but it does not fully explain why the red shift decreases with decreasing concentration. This research question was explored both theoretically and then experimentally.[15,20] The interaction of PAHs with highly orientated pyrolytic graphite (HOPG) have been theoretically modeled by Zacharia et al.[15,20] It was calculated that a graphene sheet with a coverage of less than one monolayer of a PAH (PAH having less than five rings), have a parallel orientation with the graphene surface. A coverage approaching one monolayer or greater sees the PAHs adapt an orientation with the molecular planes perpendicular (or tilted) to the surface of the graphene sheet so as to satisfy the steric and entropic constraints. These calculations were verified by spectroscopic methods such as nuclear magnetic resonance (NMR) and thermal desorption spectroscopy.[15,20] In this study a parallel orientation of *p*-terphenyl would be expressed by a red shift in the fluorescence emission spectrum whereas a perpendicular orientation would exhibit a negligible red shift.[10,18] AFM studies described in the literature[6] and in this paper show that the SWNT bundle size decreases with decreasing concentration; therefore changes in the bundle surface area may affect the alignment of *p*-terphenyl at different concentrations. The notion of *p*-terphenyl changing orientation as a result of SWNT surface area and concentration was experimentally probed with SWNT of two different bundle surface areas. Two sets of *p*-terphenyl samples ranging in concentration from $\sim 2.5 \times 10^{-6}$ to $\sim 2.5 \times 10^{-3}$ M were prepared. To one set of samples was added 3.5 mg of SWNT, and to the second set was added 0.035 mg. AFM was used to determine the average bundle sizes of SWNT in solution at the different weights and results revealed a bundle size of $\sim$23 nm for 3.5 mg and $\sim$10 nm for 0.035 mg. In this experiment the bundle size was approximately constant and the *p*-terphenyl concentrations were varied to allow one to observe the effect of the bundle size on the orientation of *p*-terphenyl molecules when an interaction takes place. In Figure 6 the results depict that the *p*-terphenyl molecules in sample

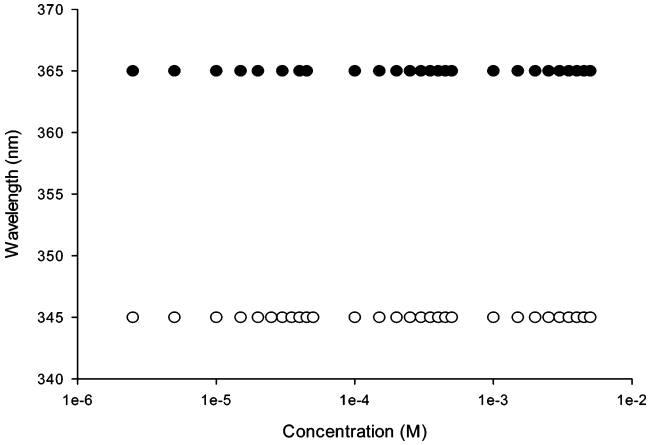

Figure 6. Fluorescence red shift of *p*-terphenyl as a function of concentration in the presence of 3.5 mg of SWNT with an average bundle size of ∼23 nm (black circles) and 0.035 mg of SWNT with an average bundle size of ∼10 nm (clear circles).

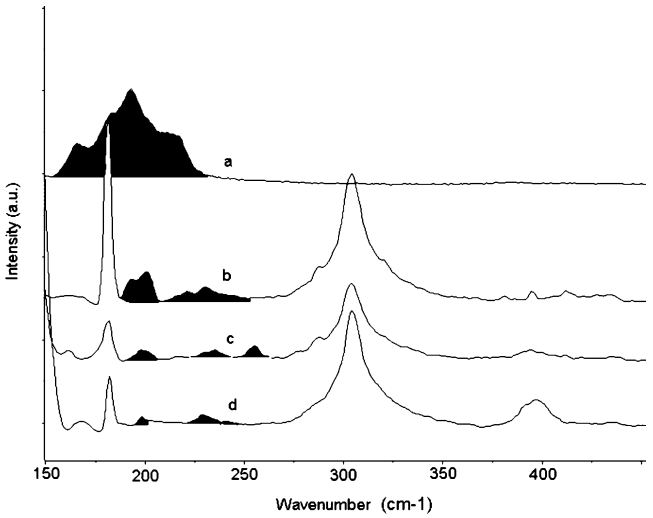

Figure 7. Radial breathing mode Raman spectra at 632.8 nm: (a) pristine SWNT; (b) composite spectrum of SWNT and anthracene at 1×10^{-6} M; (c) (b) at 1×10^{-7} M; (d) (b) at 1×10^{-8} M.

set one (filled circles) containing SWNT with an average bundle size of ∼23 nm are all red-shifted, suggesting a parallel orientation of *p*-terphenyl. In sample set two (clear circles), which contains SWNT with an average bundle size ∼10 nm, a negligible red shift was observed, suggesting a perpendicular orientation of *p*-terphenyl on interaction. Reducing the SWNT bundle size from ∼23 to ∼10 nm means that there will be an increased level of crowding of *p*-terphenyl at similar concentrations. As reported by Zacharia et al., sufficient crowding PAH on a graphene surface results in the molecules adapting a perpendicular orientation. The results from Figure 6 confirm that the SWNT bundle surface area affects the orientation of *p*-terphenyl on interaction, thus providing an explanation to the decrease in red shifting with decreasing concentration observed in Figure 5.

Raman scattering is a valuable tool to investigate the vibrational properties and thus characterize a sample of SWNT.[21] Figures 7a and 8a show two typical Raman peaks for a SWNT bundle in the ranges 100−450 and 1000−1800 cm^{-1} taken with a 632.8 nm laser excitation line. There are two phonon modes that give a strong Raman scattering signal:[22] one being the radial breathing modes (RBMs) in the region of ∼200 cm^{-1} (Figure 7a) and the second being the tangential carbon stretching modes (G-line) at ∼1580 cm^{-1} (Figure 8a). In the RBM region, the

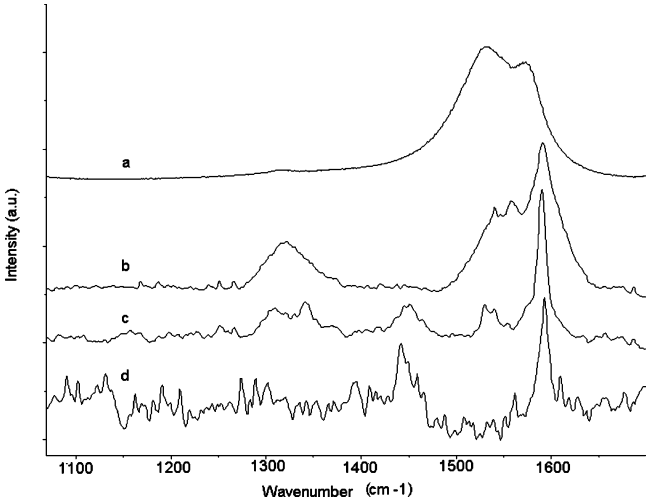

Figure 8. Raman spectra at 632.8 nm: (a) pristine SWNT; (b) composite spectrum of SWNT and anthracene at 1×10^{-6} M; (c) (b) at 1×10^{-7} M; (d) (b) at 1×10^{-8} M.

carbon atoms undergo a uniform radial displacement and experimental data confirm that the diameter of a SWNT can directly be estimated from the RBM frequency, as the two are inversely related.[22,23] The tangential mode weakly depends on diameter. Its line shape depends strongly on whether the tube is metallic or semiconducting.[21−24]

In previous work it was observed that the RBM upshifted by 6 cm^{-1} when comparing a pristine SWNT sample to the composite anthracene sample (3×10^{-4} M).[10] The upshift and the profile changes of the RBM were believed to be indicative of debundling.[25−27] The profile of the RBMs in SWNT has been shown to be dependent on the local environment and the resonant conditions.[28,29] Indeed, the resonant conditions have been shown to be dependent on the environment and can be influenced by binding and potentially the nanotube substrate environment.[29] Thus binding and substrate may affect changes in the profile through shifting of the frequencies.

Comparing these results to Figure 7 and AFM results discussed above, one may now deduce that SWNT are at most partially debundled. Further dilutions of the composite sample should effectively lead to a further upshift in the RBMs. Figure 7 compares the RBM Raman spectra of the pristine SWNT in Figure 7a, with the composite spectra at 1×10^{-6} M in Figure 7b, 1×10^{-7} M in Figure 7c and 1×10^{-8} M in Figure 7d derived from anthracene and SWNT taken at laser excitation 632.8 nm. It is important to note that some of the peaks observed in Figure 7 are due to the activated silicon substrate, for example 300, 521, and cm^{-1}, the anthracene molecule at 150, 286, and 400 cm^{-1} and the APTES at 180 cm^{-1}. To clarify the areas of interest in Figures 7 and 9, the appropriate peaks have been shaded. In Figure 7a the central positioning of the RBM for the pristine SWNT is ∼192 cm^{-1}, and consequently, it was found that, as the concentration decreases in the composite samples, the RBM upshift and appear to separate. In Figure 7b at 10^{-6} M three distinct RBM are present, at ∼198, ∼220 and ∼230 cm^{-1}. In Figure 7c at 10^{-7} M three RBM are clearly visible, at ∼198, ∼235 and ∼254 cm^{-1}. Comparing Figure 7b and Figure 7c reveals that the feature at ∼198 cm^{-1} is less intense when the concentration is decreased and the features at 220 and 230 cm^{-1} in Figure 7b have both upshifted by 15 cm^{-1} and their intensity has increased. In Figure 7d at 10^{-8} M three RBM are again present at 198, 235 and 250 cm^{-1}. Comparing Figure 7c and Figure 7d one sees that there is no further upshift and RBM are in the same region as they were in Figure 7c at

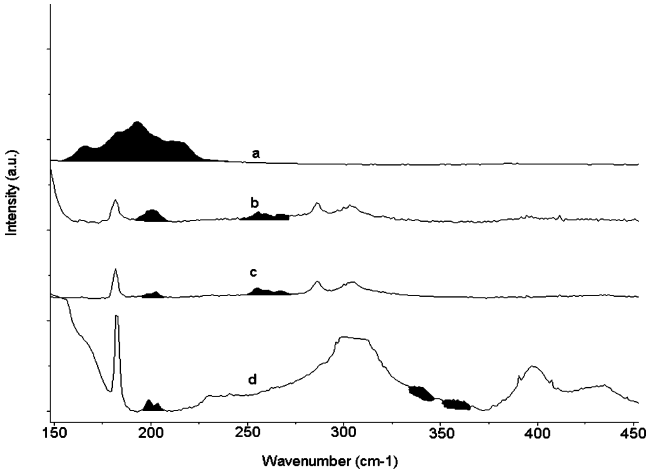

Figure 9. Radial breathing mode Raman spectra at 632.8 nm: (a) pristine SWNT; (b) composite spectrum of SWNT and *p*-terphenyl at 1×10^{-6} M; (c) (b) at 1×10^{-7} M; (d) (b) at 1×10^{-9} M.

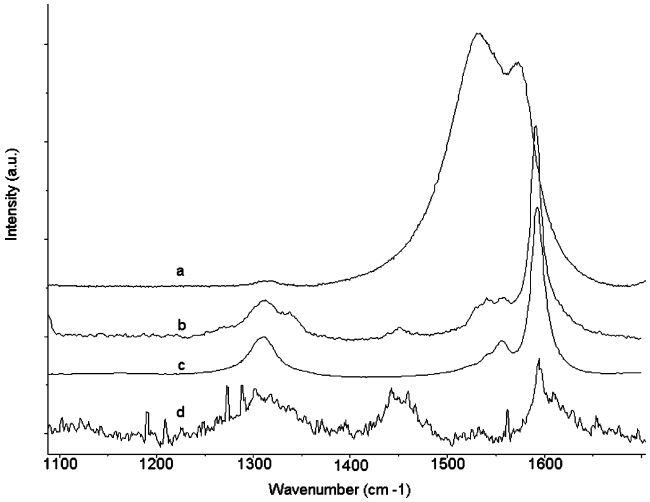

Figure 10. Raman spectra at 632.8 nm: (a) pristine SWNT; (b) composite spectrum of SWNT and *p*-terphenyl at 1×10^{-6} M; (c) (b) at 1×10^{-7} M; (d) (b) at 1×10^{-9} M.

1×10^{-7} M. This may be indicative that the SWNT are completely dispersed so that only individual SWNT exist. The result correlates with the plot of the fraction of free anthracene in Figure 4. The upshift observed is very significant as it adds further weight to the notion of SWNT debundling with decreasing concentration. From Figure 7 it would appear that the SWNT are completely dispersed at $\sim 1 \times 10^{-7}$ M (Figure 7c) as the SWNT cease to upshift further and also it would appear that once dispersed the anthracene molecules interact with SWNT of specific diameter. The upshift was calculated to be 62 cm $^{-1}$ in total on going from the pristine sample in Figure 7a to 1×10^{-7} M in Figure 7c.

Comparing Figure 8a with Figure 8b−d, the characteristic SWNT mode at 1570 cm^{-1}, the G-line, shows an upshift from 1570 to 1592 cm^{-1} on going from the pristine sample in Figure 8a to 1×10^{-7} M in Figure 8c of the composite sample. The initial G-line shape of Figure 8a has changed from metallic in nature to a more narrow and sharp peak characteristic semiconducting SWNT.[30,31] It is worth noting that both metallic and semiconducting G-lines were observed for anthracene composite samples at concentrations as low as 1×10^{-5} M and below this concentration only narrow sharp G-lines with weak intensities relative to the RBM are observed. On dispersion of SWNT it was found that the relative intensities of the G-line and RBM are inverted as Raman spectra of bundles of SWNT show a higher intensity for the G-line relative to the RBM. As the concentration decreases and SWNT disperse, the intensity ratio of the G-line to the RBM changes so that in the region where isolated SWNT are believed to exist the intensity of the RBM is greater than that of the G-line. The enhanced intensity of the RBM at the lower concentrations may be due to the release of strain imposed by bundles of SWNT[31] and various authors have also witnessed and reported similar occurrences.[32,33]

Similar behavior is observed for the *p*-terphenyl composite samples ranging from 1×10^{-6} to 1×10^{-9} M, as shown in Figures 9 and 10. The composite spectrum at 1×10^{-6} M in Figure 9b depicts the RBMs at ∼198, ∼218, ∼258, and ∼284 cm^{-1}. RBMs at 1×10^{-7} M in Figure 9c are ∼221, ∼258 and ∼284 cm^{-1}. At 1×10^{-9} M in Figure 9d the RBMs further upshift to ∼338 and ∼360 cm^{-1}. The observation of high wavenumber RBM frequencies at ∼338 and ∼360 cm^{-1} is not uncommon and authors such as Kulovecz et al. observed RBM with wavenumbers within this region.[26] The total upshift calculated from the pristine material in Figure 9a to 1×10^{-9} M in Figure 9d in the *p*-terphenyl composite material is ∼168 cm^{-1}.

Figure 10 shows the G-line for pristine SWNT (Figure 10a) and *p*-terphenyl composite samples (Figure 10b−d). As with Figure 8, the G-line upshifts with decreasing concentration and the peak once again become narrow and sharp. Papers reviewed show isolated SWNT with narrow sharp G-lines with weaker intensities relative to the RBM and these findings provoke the question of whether the Breit−Wigner−Fano (BWF) line shape observed for what is believed metallic SWNT is exclusive to bundles because such a line shape has not been observed when isolated SWNT are subject to investigation.[34] Adding support to this notion is the fact that the G-line upshifts with decreasing concentration, indicating that the bundle may impose a strain on the G-line.

Comparing the isolated SWNT solubilized by *p*-terphenyl and anthracene it would appear that the PAH molecules are indeed selective. Anthracene preferentially solubilizes larger SWNT compared to *p*-terphenyl on the basis of the accepted relationship of RBM frequency and diameter. The next stage is to try and elucidate the diameter of SWNT selected by the specific PAHs and determine the SWNT physical properties. It is well documented that the RBM wavenumber is related to the SWNT diameter and chirality but the formula to elucidate this is under debate.[31−33,35−37] The models of Jorio et al. and Rols et al. were used to determine the diameters of the SWNT.[35,37] For the anthracene composite at a concentration of $\sim 1 \times 10^{-7}$ M the υ_{RBM} of ∼198, ∼235, ∼254 cm^{-1} gave diameters of ∼1.26, ∼1.06, and ∼0.98 nm, respectively, in accordance with Jorio et al.'s. model. The diameters were estimated at ∼1.21, ∼1.02, and ∼0.95, respectively, for Rols et al.'s, model. For the *p*-terphenyl composite at a concentration of $\sim 1 \times 10^{-9}$ M Jorio et al.'s, model relates the υ_{RBM} of ∼198, ∼338, and ∼360 cm^{-1} to diameters of ∼1.26, ∼0.74, and ∼0.69 nm, respectively. According to Rols et al., the diameters are ∼1.21, ∼0.71, and ∼0.67, respectively. Comparing the resulting diameters from the two models it would appear that there is a difference in the range 0.05−0.02 nm. The difference in the diameter values only becomes significant to this work if the diameters estimated conflict with the physical properties assigned from the model to the SWNT at the given diameter, but no such disagreement occurred in this study.[35] The model of Jorio et al., is unique in that it was contrived from the study of isolated SWNT unlike other models contrived from the study of bundled SWNT.[35,38]

Therefore it is more accurate to assign SWNT properties with Jorio et al's., model as opposed to the latter model.[34,37] The results indicate that anthracene interacts with metallic SWNT whereas *p*-terphenyl interacts mainly with semiconducting SWNT. This is significant in that it indicates selective interaction of the PAH molecules with isolated SWNT. It was previously proposed that the PAH molecules anthracene and *p*-terphenyl may potentially interact with specific SWNT due to their differing backbone structure. Anthracene was proposed to map onto metallic SWNT and *p*-terphenyl to mainly semiconducting SWNT[10] and results given in this paper appear to support this proposal of commensurate π-stacking.

Conclusion

The small PAH molecules, anthracene and *p*-terphenyl have been shown to solubilize, purify, debundle and selectively interact with SWNT in toluene. The solutions are stable for prolonged periods of time. The spectroscopic investigations such as fluorescence and Raman point toward a mapping of the PAHs onto the SWNT surface. Fluorescence concentration dependence studies showed areas where aggregates of SWNT and PAHs as well as isolated SWNT and PAHs were interacting. Quenching in the fluorescence of the PAH molecules on introduction of SWNT points toward interaction, and the resulting changes in the degree of red shifting of *p*-terphenyl indicates the orientation of the PAHs and the influence of the SWNT bundle size on interaction. It was also found that the region at which the SWNT bundles disperse to give isolated SWNT is not a constant but is a three-way system dependent on the solvent used and the method by which the SWNT are produced and the molecule used to disperse the SWNT. These factors must be considered when direct comparisons of different systems are being made.

Raman spectroscopy showed composite spectra with the characteristic SWNT modes such as the RBM and the G-line upshifted in wavenumber on going from the pristine material to the composite material. Upshifting of the composite RBM compared to the pristine SWNT sample was indicative of debundling. Examination of the Raman RBM and the fluorescence of the free PAHs would appear to show that the results from both spectroscopic methods correlate when determining the region at which isolated SWNT and PAHs are interacting. Results show that anthracene debundles SWNT at $\sim 10^{-7}$ M and *p*-terphenyl at $\sim 10^{-9}$ M. Binding energies for both composite samples were obtained and found to be 1.68 and 1.46 eV for *p*-terphenyl and anthracene, respectively. Such a result indicates that *p*-terphenyl binds more tightly to the SWNT surface than anthracene but anthracene is more prolific at dispersing SWNT bundles. Raman studies were then used to probe for selective interaction of the PAHs with SWNT in the region where isolated SWNT and PAHs were believed to exist. It was found that anthracene preferentially interacted with metallic SWNT whereas *p*-terphenyl preferentially interacted with mainly semiconducting SWNT, hence providing evidence of selective interaction. Therefore it may be deduced that the PAH molecules solubilize, purify, debundle and selectively interact with specific SWNT as initially proposed.

Acknowledgment. The Focas Institute is funded under the Irish Government National Development Plan 2000−2006 with assistance from the European Regional Development Fund.

Note Added after ASAP Publication. This article was published on the Web 2/10/2006 with two incorrect values in the ninth paragraph of the Results and Discussion section. The corrected version was reposted 2/22/2006.

References and Notes

(1) Baughman, R. H.; Zakhidov, A. A. *Science* **2002**, *297*, 787.
(2) Hamada, N.; Sawada, S.; Oshiyama, S. *Phys. Rev. Lett.* **1992**, *68*, 1579.
(3) Javey, A.; Guo, J.; Farmer, D. B.; Wang, Q.; Yenilmez, E.; Gordon, R. G.; Lundstrom, M.; Dai, H. *Nano Lett.* **2004**, *4*, 1319−1322.
(4) McEuen, P. L. Single Wall Carbon Nanotubes. *Phys. World* **2000**, *13*, 31.
(5) Cadek, M.; Coleman, J. N.; Ryan, K. P.; Nicolosi, V. *Nano Lett.* **2004**, *4*, 353.
(6) Coleman, J. N.; Maier, S.; Fleming, A.; O'Flaherty, S.; Minett, A.; Ferreira, M. S.; Hutzler, S.; Blau, W. J. *J. Phys. Chem. B* **2004**, *108*, 3446.
(7) Strong, K. L.; Anderson, D. P.; Lafdi, K.; Kuhn, J. N. *Carbon* **2003**, *41*, 1477.
(8) Thess, A.; Lee, R.; Nikolaev, P.; Dai, H.; Petit, P.; Robert, J.; Xu, C.; Lee, Y. H.; Kim, S. G.; Rinzler, A. G.; Colbert, D. T.; Scuseria, G. E.; Tomanek, D.; Fisher, J. E.; Smalley, R. E. *Science* **1996**, *273*, 483.
(9) Tomanek, D. *Enbody, Science and application of Nanotubes*; Kluwer Academic Publishers: Dordrecth, The Netherlands, 2000; pp 300−302.
(10) Hedderman, T. G.; Keogh, S. M.; Chambers, G.; Byrne, H. J. *J. Phys. Chem B* **2004**, *108* (49), 18860.
(11) Walzer, K.; Sternberg, M.; Hietschold, M. *Surf. Sci.* **1998**, *415*, 376.
(12) Lateef, S. S.; Boateng, S.; Hartman, T. J.; Crot, C. A.; Russell, B.; Hanley, L. *Polym. Marer. Sci. Eng.* **2001**, *85*, 403.
(13) Uttamchandani, M.; Chen, G. Y. J.; Lesaicherre, M.; Yao, S. Q. *Bioorg. Med. Chem. Lett.* **2005**, *15*, 2447.
(14) Chakarova, S.; Schroder, E. *J. Chem. Phys*. **2005**, *122*, 054102.
(15) Zacharia, R.; Ulbricht, H.; Hertel, T. *Phys. Rev. B* **2004**, *69*, 155406.
(16) Lee, N. K.; Kim, S. K. *J. Chem. Phys*. **2005**, *122*, 031102.
(17) Hedderman, T. G.; Keogh, S. M.; Chambers, G.; Byrne, H. J. To be submitted.
(18) Cote, M.; Haynes, P. D.; Molteni, C. *Phys. Rev. B* **2001**, *63*, 125207.
(19) Coleman, J. N.; Blau, W. J.; Dalton, A. B.; Munoz, E.; Collins, S.; Kim, B. G.; Razal, J.; Selvidge, M.; Vieiro, G.; Baughman, R. H. *Appl. Phys. Lett.*, **2003**, *82*, 1682.
(20) Meehan, P.; Rayment, T.; Thomas, R. K. *J. Chem. Soc., Faraday I* **1980**, *76*, 2011−2016.
(21) Rao, A. M.; Richter, E.; Bandow, S.; Chase, B.; Eklund, P. C.; Williams, K. A.; Fang, S.; Subbaswamy, K. R.; Menon, M.; Thess, A.; Smalley, R. E.; Dresselhaus, G.; Dresselhaus, M. S. *Science* **1997**, *275*, 187.
(22) Kuzmany, H.; Plank, W.; Hulman, M.; Kramberger, Ch.; Gruneis, A.; Pichler, Th.; Peterlik, H.; Kataura., H.; Achiba, Y. *Eur. Phys. J. B* **2001**, *22*, 307.
(23) Pimenta, M. A.; Marucci, A.; Empedocles, S. A.; Bawendi, M. G.; Hanlon, E. B.; Roa, A. M.; Eklund, P. C.; Smalley, R. E.; Dresselhaus, G.; Dresselhaus, M. S. *Phys. Rev. B* **1998**, *58*, 16016.
(24) Duesberg, G. S.; Blau, W. J.; Byrne, H. J.; Muster, J.; Burghard, M.; Roth, S. *Chem. Phys. Lett*. **1999**, *310*, 8.
(25) Shui, Z.; Lian, Y.; Zhou, X.; Gu, Z.; Zhang, Y.; Iijima, S.; Gong, Q.; Li, H.; Zhang, S. *Chem. Commun.* **2000**, 461.
(26) Kataura, H.; Kumazawa, Y.; Maniwa, Y.; Umezu, I.; Suzuki, S.; Ohtsuka, Y.; Achiba, Y. *Synth. Met.* **1999**, *103*, 2555.
(27) Kulovecz, A.; Kramberger, Ch.; Georgakilas, V.; Prato, M.; Kuzmany, H. *Eur. Phys. J. B* **2002**, *28*, 223.
(28) Rao, A. M.; Chen, J.; Richter, E.; Schlecht, U.; Eklund, P. C.; Haddon, R. C.; Venkateswaran, U. D.; Kwon, Y. K.; Tomanek, D. *Phys. Rev. Lett*. **2001**, *86*, 3895.
(29) Fatini, C.; Jorio, A.; Souza, M.; Strano, M. S.; Dresselhaus, M. S.; Pimenta, M. A. *Phys. Rev. Lett*. **2004**, *93*, 147406−1.
(30) Yu, Z.; Brus, L. *J. Phys. Chem. B* **2001**, *105*, 1123.
(31) Bachilo, S. M.; Strano, M. S.; Kittrell, C.; Hauge, R. H.; Smalley, R. E.; Weisman, R. B. *Science* **2002**, 298.
(32) Keogh, S. M.; Hedderman, T. G.; Gregan, E.; Farrell, G.; Chambers, G.; Byrne, H. J. *J. Phys. Chem. B* **2004**, *108*, 6233.
(33) Pfeiffer, R.; Kuzmany, H.; Kramberger, Ch.; Schaman, Ch.; Pichler, T.; Kataura, H.; Achiba, Y.; Kurti, J.; Zolyomi, V. *Phys. Rev. Lett*. **2003**, *90*, 225501.
(34) Bandow, S.; Asaka, S.; Saito, Y.; Rao, A. M.; Grigorian, L.; Ricther, E.; Eklund, P. C. *Phys. Rev. Lett*. **1998**, *80*, 3779.
(35) Jorio, A.; Saito, R.; Hafner, J. H.; Lieber, C. M.; Hunter, M.; McClure, T.; Dresselhaus, G.; Dresselhaus, M. S. *Phys. Rev. Lett*. **2001**, *86*, 1118.
(36) Kurti, J.; Kuzmany, H.; Burger, B.; Hulman, M.; Winter, J.; Kresse, G. *Synth. Met.* **1999**, *103*, 2508.
(37) S. Rols, S.; Righi, A.; Alvarvez, L.; Anglaret, E.; Almairac, R.; Journet, C.; Bernier, P.; Sauvajol, J. L.; Benito, A. M.; Maser, W. K.; Munoz, E.; Martinez, M. T.; de la Fuente, G. F.; Girard, A.; Ameline, J. C. *Eur. Phys. J. B* **2000**, *18*, 201.
(38) Wang Y. F.; Cao, X. W.; Hu, S. F.; Liu, Y. Y.; Lan, G. X. *Chem. Phys. Lett*. **2001**, *336*, 47.